Large eddy simulation of an onshore wind farm under different operating regimes including topographic effects

M Draper[1], B López[1], D Maiuri[2], C Decaro[2], F Campagnolo[3]

[1]Grupo de Mecánica de los Fluidos Computacional, Instituto de Mecánica de los Fluidos e Ingeniería Ambiental, Facultad de Ingeniería, Universidad de la República, Uruguay.
[2]Administración Nacional de Usinas y Trasmisiones Eléctricas (UTE), Uruguay.
[3]Wind Energy Institute, Technische Universität München, Boltzmannstraße 15, D-85748 Garching bei München, Germany.

E-mail: mdraper@fing.edu.uy

Abstract. High-fidelity simulations of actual wind farms with the Actuator Line Model, in a Large Eddy Simulation framework, have been performed in the past years, for both onshore and offshore sites. It has become the state of the art to simulate the wind flow through wind turbines and wind farms and it could be a powerful tool to assess the operation of actual wind farms and potential improvements. The objective of the present paper is two-fold: develop a high-fidelity numerical model of an onshore wind farm to be used to assess the influence of different environmental and aerodynamic conditions in its power performance and analyze, as case study, the effect of the topography in the wind flow and power production.

1. Introduction

High-fidelity simulations of actual wind farms with the Actuator Line Model (ALM) [1], in a Large Eddy Simulation (LES) framework, have been performed in the past years, for both onshore and offshore sites (see for instance [2, 3, 4, 5]). It has become the state of the art to simulate the wind flow through wind turbines and wind farms and it could be a powerful tool to assess the operation of actual wind farms and potential improvements. For a comprehensive review please see [6, 7].

In the ALM the flow around the blades is not resolved as the blades are represented in the computational domain by a body force field computed from the local wind velocity and the aerodynamic coefficients, that rotates according to the rotor angular speed. Despite almost 20 years from the first publication, in the past few years there have been several proposals to improve it and new proposals are still presented [8, 9, 10, 11, 12], mostly related to the force projection. Recently, the ALM has been used to assess different operational conditions and their influence in power production and wind turbine lifetime and potential improvements.

Regarding the influence of the topography in the wakes and power production, the literature has been focused mainly in complex terrain, analyzing canonical cases, both through wind tunnel experiments and numerically [13]. Concerning the latter, in [14] Reynolds-Averaged Navier Stokes (RANS) simulations with the Actuator Disk Model (ADM) of a wind farm located in complex terrain are performed with two computational fluid dynamics (CFD) codes and a

linearized commercial software. The authors highlight that the wind fields obtained with the two CFD codes when simulating the flow over the terrain without wind turbines are similar, but the results are quite different when including them, mostly related to the way the reference wind speed of the ADM is computed. In addition to this, the authors simulated a stand-alone wind turbine placed over a flat terrain, an axisymmetric hill and a quasi-3D Gaussian hill, at the hill top. It is observed that the velocity deficit is larger in the latter cases with respect to the flat terrain and the wake center is closer to the terrain surface. The authors in [15] analyzed the effect of the terrain as well as the presence of the wind turbines wakes on the wind flow. To accomplish that, RANS simulations of the wind flow over a very complex terrain are performed, where a cluster of four wind turbines are located. The authors included in the simulations one or four wind turbines, through the ADM, with/without the terrain under two inflow conditions, aiming to isolate each effect (wakes and terrain). From the results, it can be observed that the wake of the upstream wind turbine is distorted by the terrain in an opposite direction compared to the effect of the presence of the other wind turbines, while the relative importance of the two effects depends on the inflow wind speed (thrust coefficient). A RANS approach is also used in [16], while the authors in [17] perform RANS simulations with the ADM to compute the wind flow as well as power production for a wind farm of 25 wind turbines located in complex terrain and LES-ALM simulations considering just one wind turbine using a finer spatial resolution. The authors compared the power production and angular velocity of the rotor, as well as the wind speed at two met masts, with data from the Supervisory Control and Data Acquisition systema (SCADA), for different inflow conditions. LES-ALM simulations are performed in [18] of a wind farm of 60 wind turbines in complex terrain, assessing the mean power production and power fluctuations. Several authors have analyzed canonical cases through LES showing a complex interaction between wakes and the wind flow casued by hills (see for instance [19, 20]).

The main objective of the present paper is to develop a high-fidelity numerical model of an onshore wind farm to be used to assess the influence of different environmental and aerodynamic conditions in its power performance. As case study, the effect of a non-complex topography is evaluated. The paper is organized as follows: section 2 presents briefly the selected wind farm, section 3 describes the methodology and section 4 presents the main results, while conclusions are given in section 5. This work has been done within a research project between UTE and UdelaR and it is supported by UTE-UdelaR fund.

2. Case study

An onshore wind farm in Uruguay is considered as case study. Two years of ten minutes SCADA data are used, which constitutes a new original dataset. The wind farm has not been simulated before. It is not described in detail because of a non disclosure agreement. It is composed of multi-MW wind turbines (WT), being their rotor diameter and rated power larger than 100m and 2MW respectively and tsheir rated wind speed equal to 11m/s. Two clusters of wind turbines are selected, one with 15 wind turbines (cluster A) and the other one with 10 wind turbines (cluster B). The former is used to validate the numerical model and the latter is used as case study to assess the influence of the topography in the wakes and power production. The wind farm has three met masts, one of them is selected as reference and used in the validation study, as it is close to the first cluster. The following figure depicts the wind rose as well as the mean turbulence intensity 2m below hub height and the mean wind shear exponent computed between the latter measurement height and a wind speed measurement height of 58m (close to mid-blade span), obtained from the SCADA data. Both turbulence intensity and shear exponent are computed for wind speeds larger than 3m/s. The site is characterized by a diurnal cycle, being the turbulence intensity (wind shear) larger (lower) during daytime (nightime). The wind sector influenced by neighbouring wind turbines according to annex A of IEC-61400-12-1 are represented by a grey region.

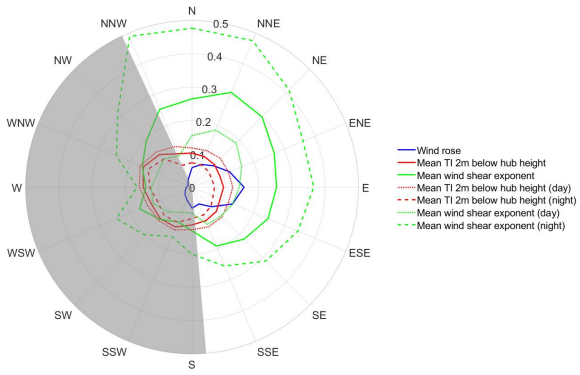

Figure 1: Wind rose (blue), mean turbulence intensity 2m below hub height (red) and mean wind shear exponent (green) at met mast, computed from 2 years of SCADA data. The mean turbulence intensity and mean wind shear exponent computed filtering by daytime and nighttime hours are also presented as dotted and dashed lines respectively.

3. Methodology

First, the main aerodynamic characteristics of the wind turbine model are defined (airfoil, chord and twist angle at different radial sections). To accomplish that, the Blade Element Momentum (BEM) method, as presented in [21], is used, and the power curve obtained is compared with the manufacturer power curve as well as 10 minutes data of two years from the Supervisory Control And Data Acquisition system (SCADA), while keeping the rotational speed as well as the pitch angle as close as possible to the SCADA data. Once the rotor model is finished, the torque and pitch controller are defined following [22] and the available SCADA data. In the torque controller, a lookup table relating the rotational speed and the generator torque computed from the SCADA data is used. Unsteady BEM [21] simulations are run, including the rotor geometry as well as the controller, to validate the wind turbine model.

LES-ALM simulations are performed with the open source finite volume code caffa3d [23, 24], that has been validated for wind energy applications, for both wind tunnel and actual wind farm cases, [4, 5, 25], including the recently proposed limitation to the projection region of the aerodynamic forces [26]. A brief description of the numerical domain and numerical setup is given below. For further details about the numerical code and setup please see [4, 5].

For both wind turbines clusters, the numerical domain is 8km x 6km x 1km in the streamwise, spanwise and vertical direction. The streamwise and spanwise directions are uniformly divided into 496 and 372 grid cells respectively, while a stretched grid is used in the vertical direction with 126 grid cells, being 2.5m the first cell height above the surface (30 grid cells cover a vertical diameter). The simulations are run for 2600s of physical time.

Regarding the numerical setup for the LES-ALM simulations of both clusters, a zero velocity gradient is imposed at the outlet and a wall model based on the log law is used to compute the stress at the surface while periodic conditions are used in the lateral boundaries. The topography is represented by body fitted blocks of structured grids and the surface roughness is considered in the above mentioned log law. The Crank-Nicolson scheme is used to advance in time. The scale dependent dynamic Smagorinsky model with local averaging scheme is used to compute the subgrid scale stress. The convective term is approximated by an implicit term and an explicit deferred correction, combining a third order compact scheme with a fourth order central difference compact scheme [27]. The inflow conditions are obtained from precursor simulations, taking into account the same numerical setup but without wind turbines and topography while applying a periodic boundary condition in the west and east boundaries and

a constant pressure gradient as forcing term. In the precursor simulations a similar stratregy as the one presented in [28] is used to avoid locking large turbulent structures that generate statistical inhomogeneities in the spanwise direction. Figure 2 depicts the vertical profiles of the mean streamwise velocity component and the turbulence intensity. As can be seen, the turbulence intensity of the precursor simulations are close to the mean values for the main wind directions, while the shear exponents are lower than the mean value and close to the mean value during daytime. The mean streamwise velocity component at hub height are 7.0m/s, 8.1m/s, 8.8m/s, 10.3m/s and 13.3m/s (the precursor simulations are named Prec7, Prec8, Prec9, Prec10 and Prec13 respectively).

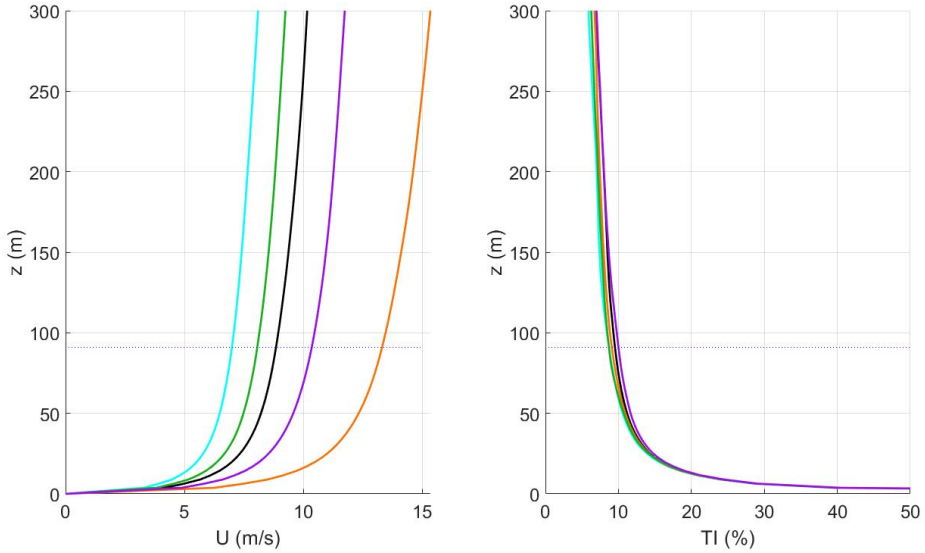

Figure 2: Vertical profile of the mean streamwise velocity component (left) and turbulence intensity (right), obtained in the precursor simulations. The hub height is represented by a blue-dotted line.

LES-ALM simulations of cluster A are performed for different inlet conditions, both wind speed profiles (obtained from the above five precursor simulations) and wind directions, as presented in table 1. The different wind directions are obtained by rotating the topography and wind turbines and keeping the west boundary as inlet boundary. The power production, rotational speed and pitch angle are compared with SCADA data in section 4.1. It should be mentioned that the SCADA data has been filtered in order to keep the records where all the wind turbines considered in the simulations are operating in normal conditions.

To evaluate the influence of the topography, LES-ALM simulations are run with/without the topography for cluster B and taking into account one precursor simulation (Prec9) and one wind direction (95^o). The wake characteristics and the wind turbine's operation are compared in section 4.2.

4. Results

4.1. Cluster A: validation of the high fidelity numerical model

One objective of the present paper is to develop a high fidelity numerical model of an onshore wind farm, particularly focused on the wind turbines operation and their power production while taking into account the interaction with the wind field. The model would be used to assess in

Table 1: Numerical simulations performed for cluster A. The mean streamwise velocity component of each precursor simulation (shown in brackets), its turbulence intensity at hub height and the shear exponent are included. RWS: rated wind speed.

Precursor simulation	Wind direction	Turbulence intensity	Shear exponent	
Prec7 (7.0m/s)	90^o	8.7%	0.13	Below RWS
Prec8 (8.1m/s)	90^o	8.7%	0.12	Below RWS
Prec9 (8.8m/s)	90^o	9.5%	0.12	Below RWS
Prec10 (10.3m/s)	90^o	10.0%	0.13	$\sim$ RWS
Prec13 (13.3m/s)	90^o	9.1%	0.13	Above RWS
Prec9 (8.8m/s)	115^o	9.5%	0.12	Below RWS
Prec9 (8.8m/s)	125^o	9.5%	0.12	Below RWS

the near future the influence of environmental factors as well as operational strategies in its power production. In this section, the main results of the simulations performed for cluster A (see table 1) are presented as validation case.

Figure 3 presents the terrain elevation of the domain considered when simulating wind direction 90^o. Figure 4 depicts the mean streamwise velocity component at hub height for a wind direction of 90^o and precursor simulations Prec7 and Prec9. This wind direction is the most frequent. The wind turbines are not heavily waked, just WT18 is waked by WT11 and to a lesser extent WT06 by WT03. As expected, the larger the terrain height, the larger the mean wind speed, despite being a relatively smooth terrain. As a result, the wind turbines placed at higher altitudes generates more power.

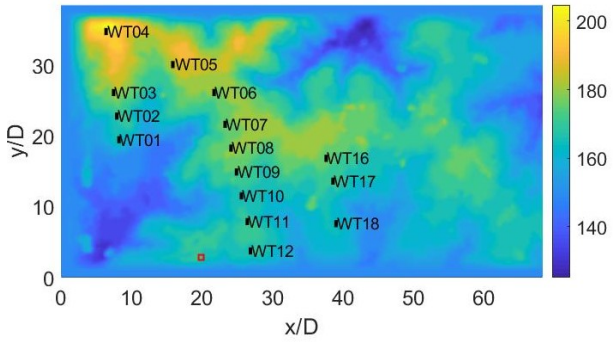

Figure 3: Terrain elevation. The met mast is represented as a red square. Wind direction: 90^o.

Regarding the wind turbines operation, to visualize the different control regimes resulting from the different wind speed profiles, figure 5 presents the power production of each wind turbine as a function of the wind speed at the met mast. The figure includes ten minutes averages of the SCADA data, filtered by wind direction measured at the met mast (wind sector width of 4^o). The simulated data is presented as ten minutes moving averages. From the figure, it can be observed that the wind turbines behaves as expected, controling its rotational speed and power production by the applied generator torque and pitching the blades. The wake effect on WT18 can be more clearly seen. While most of the wind turbines operates at rated power when Prec10 is used as inlet condition, WT18 is operating close to the power curve knee. Similar results are observed when assessing the rotational speed and the pitch angle obtained in the simulations (not shown here for brevity).

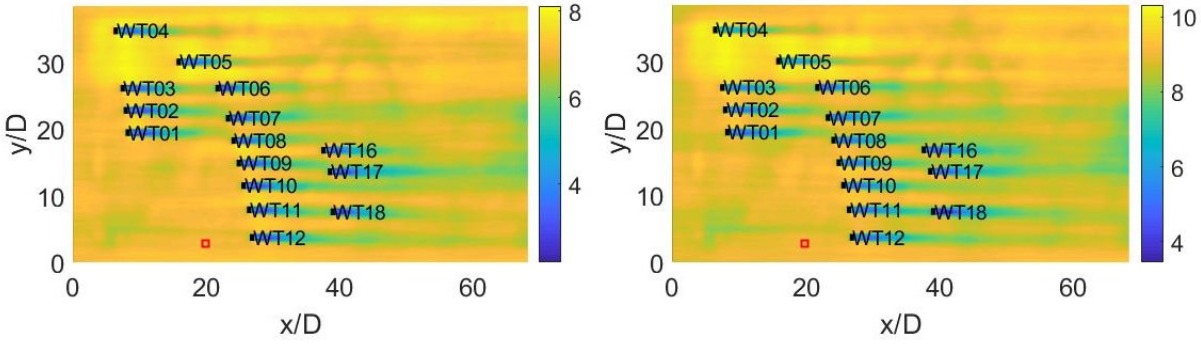

Figure 4: Mean streamwise velocity component at hub height for precursor simulations Prec7 (left) and Prec9 (right). The met mast is represented as a red square. Wind direction: 90^o.

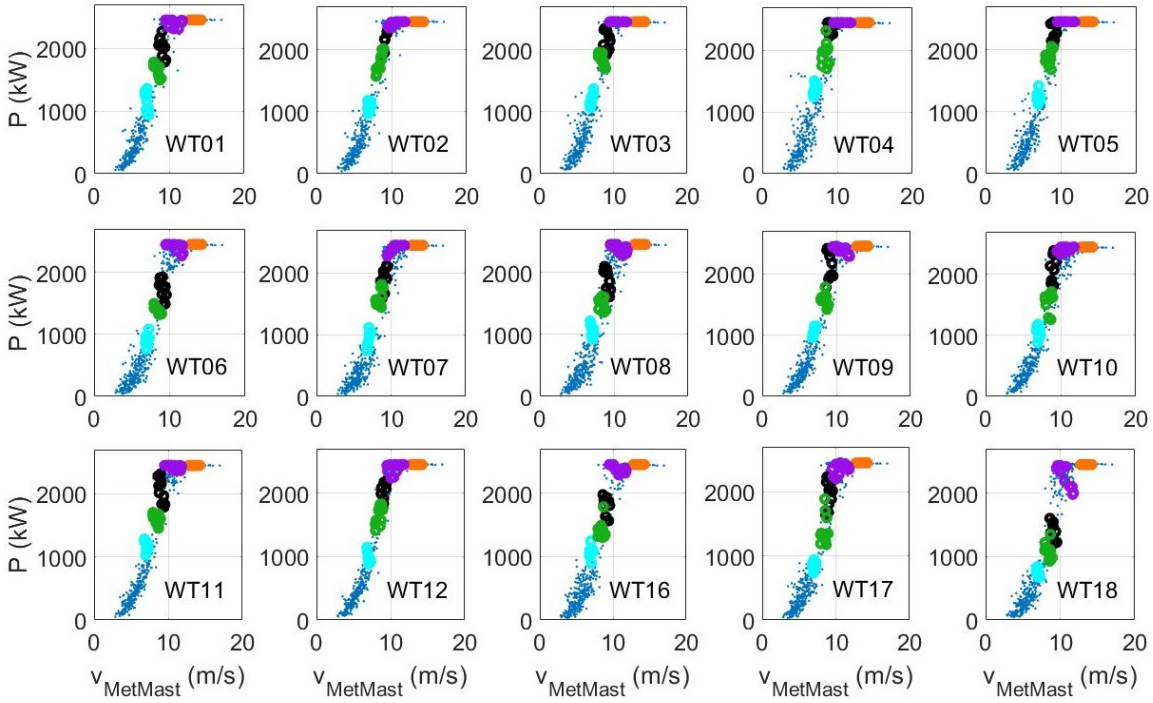

Figure 5: Generated power of each wind turbine as a function of the wind speed at the wind farm met mast. Circles: simulated results (ten minutes moving averages). Each colour represents a precursor simulation used at the inlet boundary. Blue-dots: ten minutes SCADA data. Wind direction: 90^o.

To evaluate the simulated power production, figure 6 presents a boxplot of the ten minutes averaged power production of each wind turbine from the SCADA data filtered by wind speed and wind direction measured at the met mast. The mean wind speed obtained at each simulation (different precursor simulation) at the met mast position is used to filter the SCADA data, taking into account a wind speed bin of 1m/s. In addition to this, the SCADA data is filtered by wind direction using a wind sector of 4^o. It should be mentioned that, with these filters, the number of ten minutes records considered is quite low. The wind turbines that show a power boosting due to the terrain are highlighted in green while the ones affected by the wakes of neighbouring wind turbines are highlighted in red. From the boxplot it can be observed that the general trend is well captured. WT04 produces more power while WT06 and WT07 produce less power than

the rest of the wind turbines for wind speeds 7.1m/s and 8.1m/s (Prec7 and Prec8 respectively). The transition from operating below and above rated power is captured by the simulations. For instance, for Prec9 WT04 operates at rated power and WT06 and WT07 operate below it. A similar trend is observed for Prec10, while for Prec13 all the wind turbines operate at rated power. The main difference is seen at WT18 for Prec9. A possible reason could be the difference in the inflow wind speed, particularly the turbulence intensity, associated to the SCADA records and the simulation, generating the latter a larger wake effect.

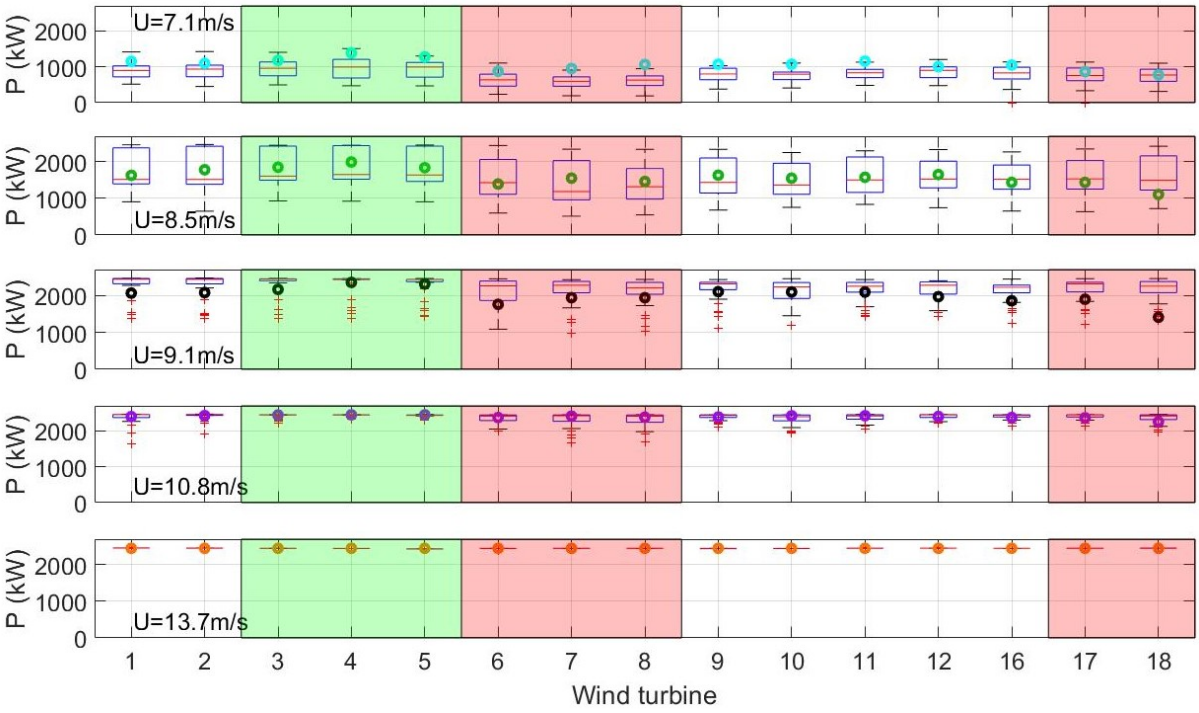

Figure 6: Boxplot of the generated power of each wind turbine filtering the SCADA data according to the wind speed at the wind farm met mast (bines width of 1m/s) and wind direction 90^o (wind sector width of 4^o). Circles: mean results from the simulations. From top to bottom, precursor simulations: Prec7, Prec8, Prec9, Prec10, Prec13. Wind direction: 90^o. The mean wind speed at the met mast is shown at the right. The green and red regions highlights the wind turbines that show a power boost due to the terrain or are affected by wakes respectively.

In order to get a deeper look at the interaction of wind turbines, two additional simulations with Prec9 where performed for wind directions 115^o and 125^o. At wind direction 115^o, WT05 is waked by WT04 and WT06 is mostly non-waked, and at wind direction 125^o WT06 is waked by WT04 and WT05 is not waked (please see figure 7). Figure 8 presents the power ratios between these three wind turbines as a function of the measured wind direction at the met mast. The SCADA data has been filtered according to the wind speed measured at the mast (between 8.5m/s and 9.5m/s). It is interesting to note that at wind direction 115^o WT06 produces more power than WT05, changing its powers ratio at 125^o. The simulations are able to capture these differences in power production.

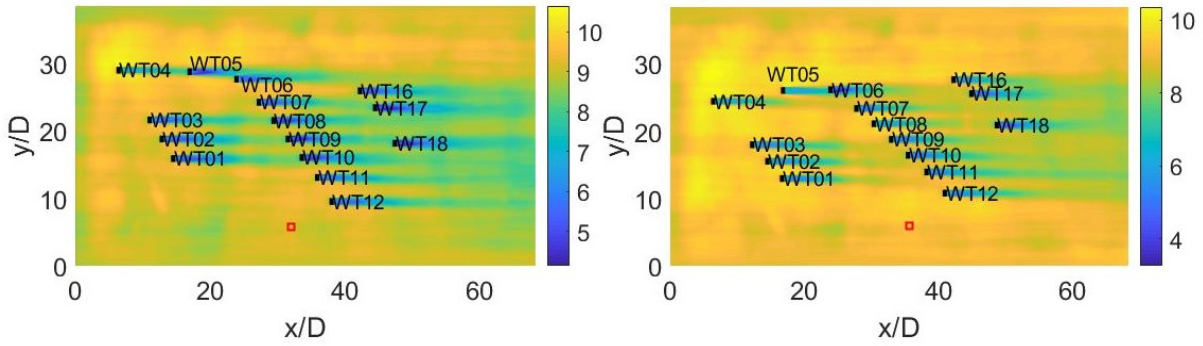

Figure 7: Mean streamwise velocity component at hub height for wind direction 115^o (left) and 125^o (right). The met mast is represented as a red square. Precursor simulation: Prec9.

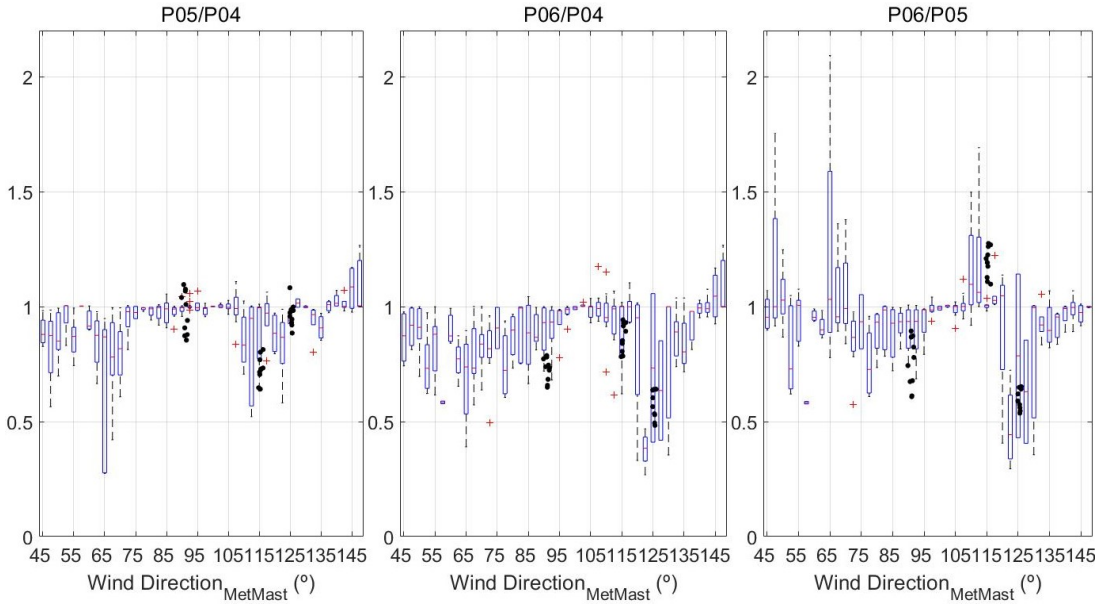

Figure 8: Ratios of generated power of wind turbines WT04, WT05 and WT06 as a function of the wind direction at the wind farm met mast. Circles: simulated results (ten minutes moving averages). Boxplots computed from ten minutes SCADA data filtered by wind speed at met mast between 8.5m/s and 9.5m/s and binned by 2.5^o wind sectors. Precursor simulation: Prec9.

4.2. Cluster B: topographic effects

In this section the effect of the topography is explored. To accomplish that, cluster B of 10 wind turbines is simulated without (flat) and with the orography (topo). This cluster of wind turbines is selected as they are placed in two lines over two regions of similar elevation and separated by a lower elevation zone, being the difference between them around 20% of the rotor diameter. In general, the influence of the topography in the wakes has been assessed for larger differences, particularly complex terrain. Nevertheless, it is interesting to evaluate how this small differences in terrain with respect to a flat one may affect the wakes and the power production. Figure 9 presents the mean streamwise velocity component at hub height for the simulation with the topography and the terrain elevation.

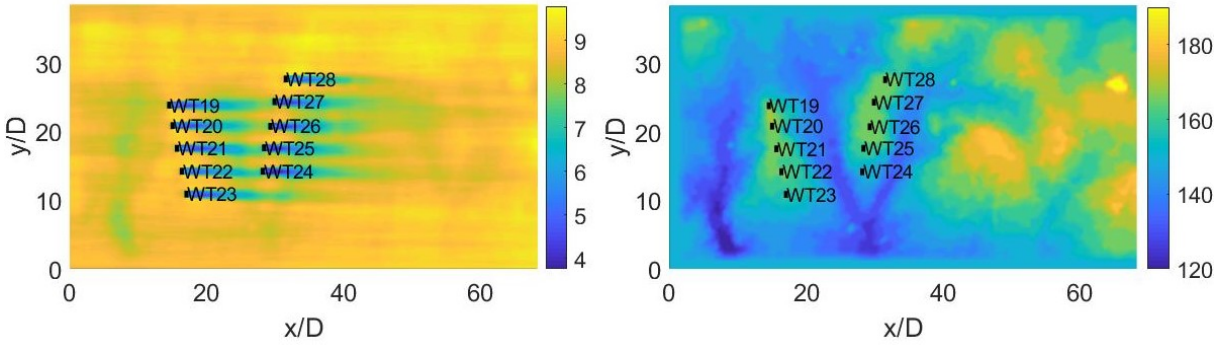

Figure 9: Mean streamwise velocity component at hub height for the simulation with topography (left) and terrain elevation (right). Wind direction: 95^o. Precursor simulation: Prec9.

Figures 10 and 11 depicts surface plots of the mean streamwise velocity component in a vertical plane passing through WT21 rotor centre for the case without and with topography. As mentioned in [13], two major effects on the flow passing above topography are produced by its presence: non-zero pressure gradient and curvature of the streamline. It can be observed that the wake of WT21 is slightly deviated. Despite the relatively smooth terrain, the wake is affected, both the velocity deficit as well as the turbulence intensity. Regarding the latter, the peak value is found at the top tip height in both cases as expected (see for example [4, 29]). This is more clear in figures 12 and 13, where the vertical profiles of the mean streamwise velocity component and turbulence intensity at different locations in the wake of WT21 are presented. The wakes at 2.1D and 3.0D downstream from the rotor plane are quite similar, while they start to deviate further downstream. The simulation with the topography presents larger velocity deficit and turbulence intensity. The wake for the case with topography seems to recover slower up to 8.0D downstream and faster further donwstream.

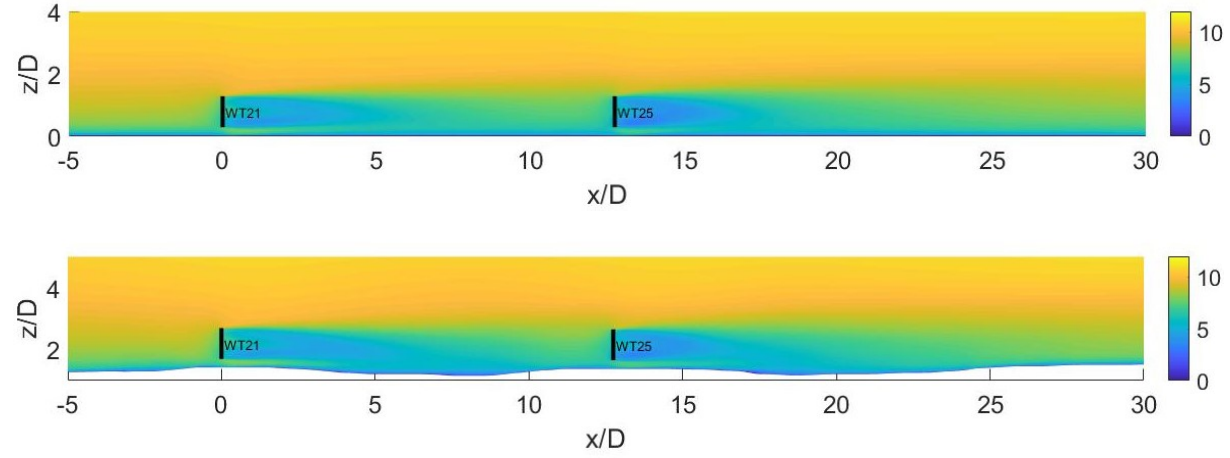

Figure 10: Mean streamwise velocity component at a vertical plane passing through the rotor centre of wind turbine WT21 for the simulation without (top) and with (bottom) topography. Wind direction: 95^o. Precursor simulation: Prec9.

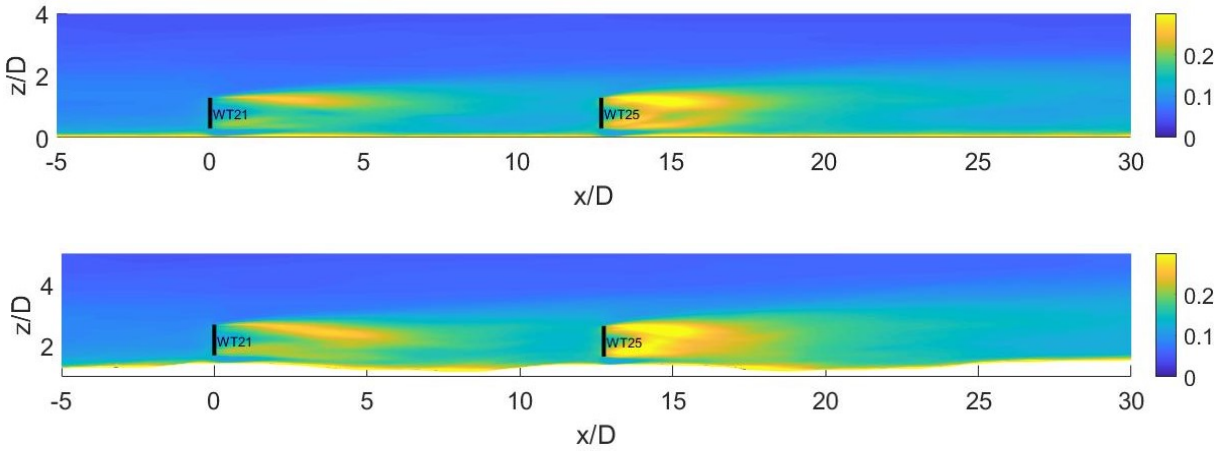

Figure 11: Streamwise turbulence intensity at a vertical plane passing through the rotor centre of wind turbine WT21 for the simulation without (top) and with (bottom) topography. Wind direction: 95^o. Precursor simulation: Prec9.

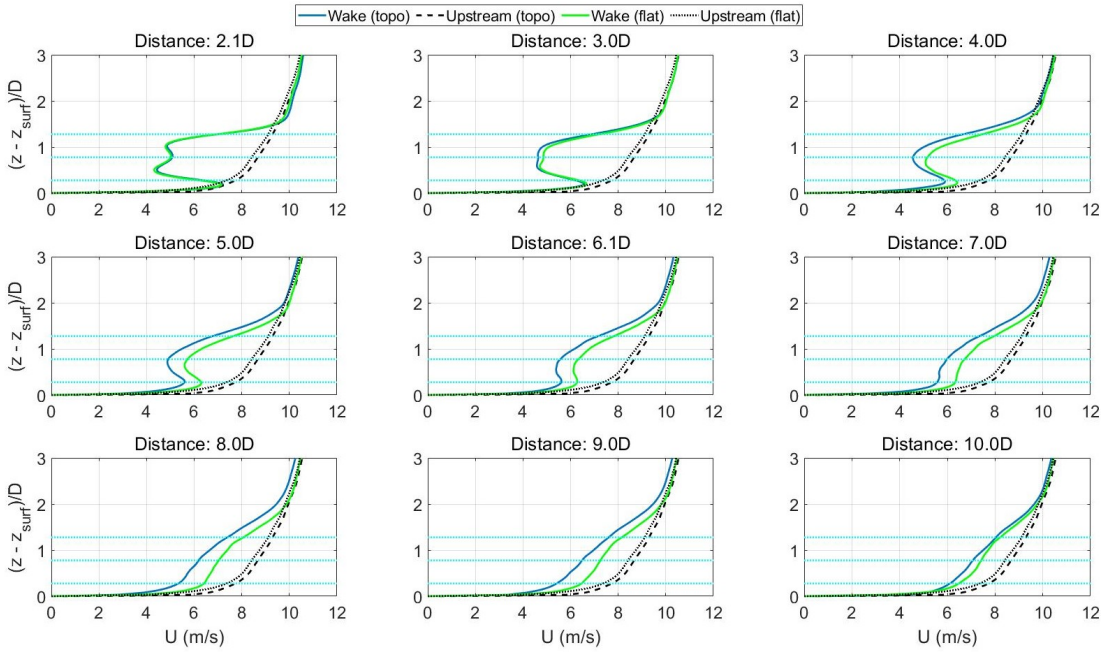

Figure 12: Vertical profiles of the mean streamwise velocity component at different positions in the wake of wind turbine WT21 for the simulation without and with topography. The vertical profile 1D upstream of WT21 is included (black dotted line: simulation without topography, black dashed line: simulation with topography). The hub and tips heights are shown as dotted cyan lines. Wind direction: 95^o. Precursor simulation: Prec9.

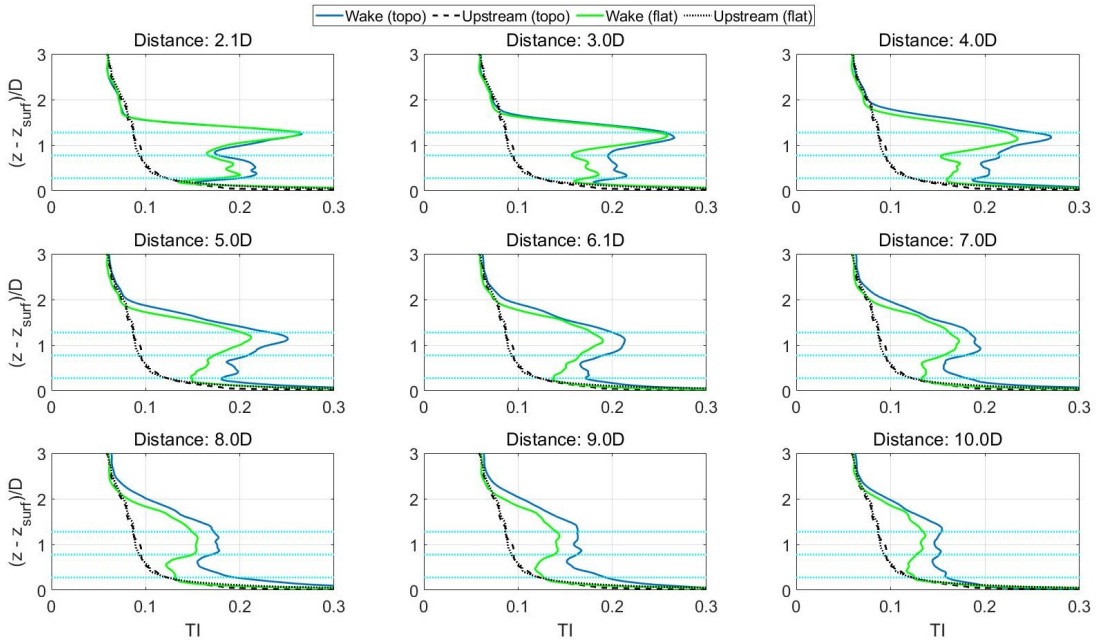

Figure 13: Vertical profiles of the streamwise turbulence intensity at different positions in the wake of wind turbine WT21 for the simulation without and with topography. The vertical profile 1D upstream of WT21 is included (black dotted line: simulation without topography, black dashed line: simulation with topography). The hub and tips heights are shown as dotted cyan lines. Wind direction: 95^o. Precursor simulation: Prec9.

Regarding the power production of cluster B, it can be seen in figure 14 that the mean power of the first line of wind turbines is larger when the topography is included in the simulation, consistent with the vertical profile observed upstream of WT21. Also, the second line of wind turbines produces more power. The wake effect between both lines is almost not affected. Probably, if the two lines were closer, the wake effect would be larger for the simulation with the topography.

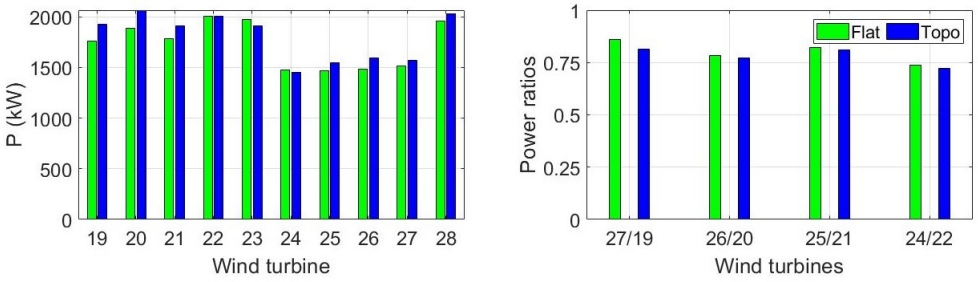

Figure 14: Mean power production (left) and ratios of mean power of the waked wind turbines (right) for the simulations without and with topography. Wind direction: 95^o. Precursor simulation: Prec9.

5. Conclusions

A numerical model of an onshore wind farm, based on the Actuator Line Model to represent the wind turbine rotor and Large Eddy Simulation method to solve the governing equation (LES-ALM), has been developed, including the aerodynamic design of the wind turbine rotor in order to match the manufacturer power curva and the available SCADA data. The developed numerical framework captures the dynamic of the operation of the onshore wind farm, as well as its interaction with the wind field. Power production, rotational speed and pitch angle

obtained in LES-ALM simulations are compared with 10 minutes SCADA data for different inlet conditions, resulting in the operation of the wind turbines under different regimes.

The numerical model is used to evaluate the influence in power production as well as wake characteristics of the topography, through simulating the same cluster of wind turbines and inlet condition with/without the topography. Despite being a smooth terrain, the wake is modified by the topography. Nevertheless, for the studied cluster of wind turbines and inlet condition considered, the wake effect is almost not affected.

Several future research lines are planned. For example, the numerical framework will be coupled with the mesoscale model WRF to simulate the operation of the onshore wind farm considering atmospheric forcings closer to the actual ones. The comparison with the SCADA data could look deeper by using 1Hz data that may be available for certain periods. On the other hand, the influence of environmental conditions, like wind speed vertical profile or turbulence intensity, will be assessed, both for a stand-alone wind turbine over different terrains as well as cluster of wind turbines. This numerical study will be complemented with the assessment of the available SCADA data. It should be noted that the research group is finishing the migration of the code to CPU-GPU infrastructure, so its computational cost will be dramatically reduced, becoming a powerful tool for academic and industrial use.

6. References

[1] Sørensen J N and Shen W Z 2002 *Journal of fluids engineering* **124** 393–399
[2] Churchfield M, Lee S, Moriarty P, Martinez L, Leonardi S, Vijayakumar G and Brasseur J 2012 *50th AIAA Aerospace Sciences Meeting including the New Horizons Forum and Aerospace Exposition*
[3] Xie S and Archer C 2015 *Wind Energy* **18** 1815–1838
[4] Draper M, Guggeri A, Mendina M, Usera G and Campagnolo F 2018 *Journal of Wind Engineering and Industrial Aerodynamics* **182** 146–159
[5] Guggeri A and Draper M 2019 *Energies* **12** 3508
[6] Sørensen J N, Mikkelsen R F, Henningson D S, Ivanell S, Sarmast S and Andersen S J 2015 *Philosophical Transactions of the Royal Society A: Mathematical, Physical and Engineering Sciences* **373** 20140071
[7] Breton S P, Sumner J, Sørensen J N, Hansen K S, Sarmast S and Ivanell S 2017 *Philosophical Transactions of the Royal Society A: Mathematical, Physical and Engineering Sciences* **375** 20160097
[8] Shives M and Crawford C 2013 *Wind Energy* **16** 1183–1196
[9] Meyer Forsting A R, Pirrung G R and Ramos-García N 2019 *Wind Energy Science* **4** 369–383
[10] Martínez-Tossas L A and Meneveau C 2019 *Journal of Fluid Mechanics* **863** 269–292
[11] Dağ K O and Sørensen J N 2020 *Wind Energy* **23** 148–160
[12] Xue F, Duan H, Xu C, Han X, Shangguan Y, Li T and Fen Z 2022 *Energies* **15** 282
[13] Shamsoddin S and Porté-Agel F 2018 *Journal of Fluid Mechanics* **855** 671–702
[14] Politis E S, Prospathopoulos J, Cabezon D, Hansen K S, Chaviaropoulos P and Barthelmie R J 2012 *Wind Energy* **15** 161–182
[15] Castellani F, Astolfi D, Mana M, Piccioni E, Becchetti M and Terzi L 2017 *Wind Energy* **20** 1277–1289
[16] Murali A and Rajagopalan R G 2017 *Journal of Wind Engineering and Industrial Aerodynamics* **162** 57–72
[17] Sessarego M, Shen W Z, Van der Laan M P, Hansen K S and Zhu W J 2018 *Applied Sciences* **8** 788
[18] Yang X, Pakula M and Sotiropoulos F 2018 *Applied energy* **229** 767–777
[19] Liu L and Stevens R J 2020 *Boundary-Layer Meteorology* **176** 251–269
[20] Liu Z, Lu S and Ishihara T 2021 *Wind Energy* **24** 857–886
[21] Hansen M O 2015 (Routledge)
[22] Jonkman J, Butterfield S, Musial W and Scott G 2009 Tech. rep. National Renewable Energy Lab.(NREL), Golden, CO (United States)
[23] Usera G, Vernet A and Ferré J A 2008 *Flow, Turbulence and Combustion* **81** 471–495
[24] Mendina M, Draper M, Soares A P K, Narancio G and Usera G 2013 *Cluster Computing* **17** 231–241
[25] Mühle F, Schottler J, Bartl J, Futrzynski R, Evans S, Bernini L, Schito P, Draper M, Guggeri A, Kleusberg E *et al.* 2018 *Wind Energy Science* **3** 883–903
[26] Draper M, López B, Guggeri A, Campagnolo F and Usera G 2020 *Journal of Physics: Conference Series* vol 1618 (IOP Publishing) p 022051
[27] Ferziger J and Peric M 2002 3rd ed (Springer-Verlag Berlin Heidelberg)
[28] Munters W, Meneveau C and Meyers J 2016 *Physics of Fluids* **28** 025112
[29] Wu Y T and Porté-Agel F 2011 *Boundary-layer meteorology* **138** 345–366